Inhomogeneous absorption of laser radiation: Trigger of LIPSS formation

J. Z. P. Skolski[*1], G. R. B. E. Römer[*2], J. V. Obona[*3], V. Ocelik[*3], A. J. Huis in 't Veld[*2,4] and J. Th. M. De Hosson[*5]

[*1] *Materials innovation institute M2i, Faculty of Engineering Technology, Chair of Applied Laser Technology,University of Twente, P.O. Box 217, 7500 AE, Enschede, The Netherlands*
E-mail: j.z.p.skolski@utwente.nl
[*2] *University of Twente, Faculty of Engineering Technology, Chair of Applied Laser Technology, P.O. Box 217, 7500 AE, Enschede, The Netherlands*
[*3] *Materials innovation institute M2i, Department of Applied Physics, University of Groningen, Nijenborgh 4, 9747 AG Groningen, The Netherlands*
[*4] *TNO Technical Sciences; Mechatronics, Mechanics and Materials, De Rondom 1, 5600 HE, Eindhoven, The Netherlands*
[*5] *University of Groningen, Department of Applied Physics, Materials Science Centre, Nijenborgh 4, 9747 AG Groningen, The Netherlands*

The finite-difference time-domain method is used to study the inhomogeneous absorption of linearly polarized laser radiation below a rough surface. The results are analyzed in the frequency domain. It is shown that laser-induced periodic surface structures, with a periodicity larger than the laser wavelength, can be understood in the frame of an electromagnetic approach.

Keywords: LIPSS, grooves, efficacy factor, FDTD, rough surfaces

1. Introduction

Laser-induced periodic surface structures (LIPSSs) have been studied since the 1960s [1] and observed on many types of materials [2]-[6], however a complete understanding of their origin and growth is still missing.

The most common LIPSSs, also referred to as ripples, consist of wavy surfaces which can be produced on metals [2]-[3], semiconductors [4]-[5], and dielectrics [6]. When created with a linearly polarized laser radiation at normal incidence, these ripples have a periodicity close to the laser wavelength and a direction orthogonal to its polarization. Ripples having these properties can be produced with either cw lasers or pulsed lasers and are usually referred to as low spatial frequency LIPSSs (LSFLs). It is generally accepted that LSFL formation is driven by the interaction of the electromagnetic field with material's rough surfaces. This phenomenon is often studied via the efficacy factor theory, also referred to as Sipe theory [7].

The observation of ripples with a periodicity significantly smaller than the laser light, referred to as high spatial frequency LIPSSs (HSFLs), renewed interest in the topic since the early 2000s [8]-[10]. HSFLs have only been observed for laser pulse durations in the picosecond and femtosecond regime. Other phenomena, such as the variation of LSFL periodicity as function of the number of pulses applied [11]-[13], or the presence of "grooves" (see Figure 1) with a periodicity larger than the laser wavelength have also been discussed recently [13]-[15]. The observation of this plethora of unexpected LIPSSs triggered mainly two kinds of theoretical explanations. The first theory is based on a careful study of the interaction of electromagnetic fields with rough surfaces [11]-[12] and more specifically the role of surface plasmon polaritons (SPPs) in LSFL formation. In the second theory, it is proposed that LIPSSs are the result of "self-organization from an instability induced by the ablation process" [16]-[17].

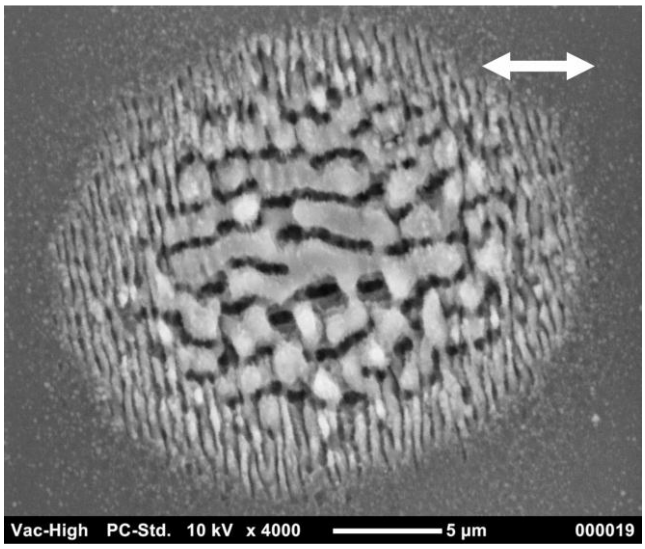

Figure 1: Scanning electron microscopy picture of LSFL (outer part) and grooves (inner part) produced on silicon with 500 pulses of a 800 nm femtosecond laser source. The white arrow indicates the polarization.

In a recent article [18], the analytical solution of the interaction of electromagnetic fields with material's rough surfaces provided by Sipe et al. [7] was compared to numerical simulations performed with the finite-difference time-domain (FDTD) method. The two approaches were

shown to be in good agreement. However, the numerical simulations show more results since they are neither limited by the approximations implied by the efficacy factor theory, nor are the results limited to the frequency domain. It was shown that the electromagnetic approach is not limited to the explanation of LSFL formation, but can, using the same model, also account for the presence of HSFLs. Additional simulations were needed to verify whether grooves could also be understood in the frame of this theory. The latter is the purpose of this paper.

To this end, first the main features and notations developed in [18] are summarized. Then, the results of FDTD simulations are presented in the frequency domain in order to get a better understanding of grooves formation.

2. FDTD simulations

The FDTD method can be applied to numerically solve Maxwell's equations. It was introduced by Yee in 1966 and gained popularity with the increase of computational power [19]. Yee's algorithm is based on the two coupled Maxwell's curl equations. In the case of linear, isotropic, nondispersive materials, with no magnetic loss, Maxwell's curl equations can be written as [20]

$$\mu_0 \frac{\partial \vec{H}}{\partial t} = -\vec{\nabla} \times \vec{E} \tag{1}$$

$$\varepsilon_0 \varepsilon_r \frac{\partial \vec{E}}{\partial t} + \sigma \vec{E} = \vec{\nabla} \times \vec{H} \tag{2}$$

where t is the time, μ_0 is the free-space permeability, ε_0 is the free-space permittivity, ε_r is the relative permittivity, σ is the electric conductivity, $\boldsymbol{E}$ is the electric field, and $\boldsymbol{H}$ is the magnetic field. In Yee's algorithm, Eqs. (1) and (2) are expressed in a Cartesian frame. To numerically evaluate the equations, central differences are used for the finite-difference expressions of the space and time derivatives. The projection of the discretized version of Eq. (1) along the x axis is, for example,

$$\begin{aligned} H_x^{n+\frac{1}{2}}\left(i, j+\frac{1}{2}, k+\frac{1}{2}\right) &= H_x^{n-\frac{1}{2}}\left(i, j+\frac{1}{2}, k+\frac{1}{2}\right) \\ &- \frac{\Delta t}{\mu_0 \Delta y}\left[E_z^n\left(i, j+1, k+\frac{1}{2}\right) - E_z^n\left(i, j, k+\frac{1}{2}\right)\right] \\ &+ \frac{\Delta t}{\mu_0 \Delta z}\left[E_y^n\left(i, j+\frac{1}{2}, k+1\right) - E_y^n\left(i, j+\frac{1}{2}, k\right)\right], \end{aligned} \tag{3}$$

where the superscript n indicates the time steps, Δt is the time increment, Δx, Δy, and Δz are the space increments, and i, j, and k are the discretized space coordinates. Each component of **E** and **H** is respectively surrounded by four circulating components of **H** and **E**. Such an arrangement is referred to as Yee cell and is used to span the simulation domain.

As in [18], the FDTD method is used to study the inhomogeneous absorption of linearly polarized laser radiation below a rough surface. The wavelength of the laser light λ was set to 800 nm in all the simulations. A slice of the simulation domain along the xz plane is represented schematically in Figure 2. The linearly polarized plane waves are introduced above the rough surface via the total-field scattered-field technique (dotted lines) [20]. The simulation domain is terminated in the z direction by two uniaxial perfectly matched layers (UPMLs), twenty Yee cells wide to avoid nonphysical reflections [21]. In the x and y directions, periodic boundary conditions were implemented (dashed lines) [20].

The number of Yee cells N_x and N_y in the x and y directions respectively were N_x=N_y=550. The number N_z of Yell cells used in the z direction depends on the number of planes used to simulate the rough surface and is mentioned in the article when appropriate. The dimensions of the Yee cells were set to Δx = 40 nm, Δy = 40 nm, Δz = 20 nm and the time increment Δt to 0.04 fs.

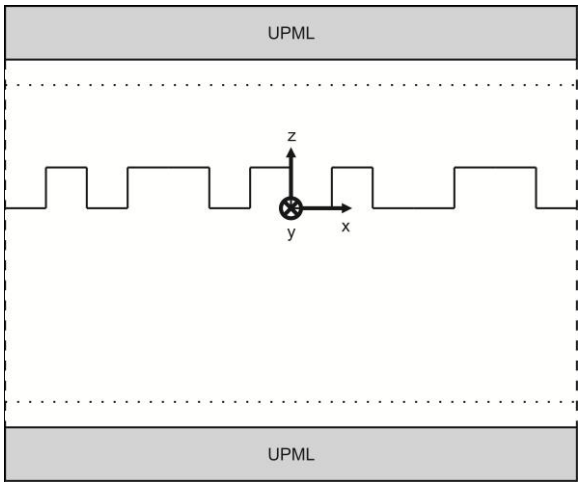

Figure 2: Schematic representation of the simulation domain. Note that the image is not to scale. Dashed lines (left and right) represent periodic boundary conditions. Dotted lines (top and bottom) are planes where the total-field scattered-field technique is used to introduce plane waves in the simulation domain.

The optical properties ε_r and σ of silicon under femtosecond excitation were calculated using the same approach as Bonse et al. [11] while these authors were testing the Sipe-Drude model. The complex permittivity of excited silicon is given by $\tilde{\varepsilon}^* = \tilde{\varepsilon} + \Delta\tilde{\varepsilon}_{Drude}$ where

$$\Delta\tilde{\varepsilon}_{Drude} = \frac{-e^2 N_e}{\varepsilon_0 m_{opt}^* m_e \omega^2 \left[1 + i(\omega\tau_D)^{-1}\right]} \tag{5}$$

Here, e, N_e, m_{opt}^*, m_e, ω, and τ_D denote the electron charge, the electron density in the conduction band, the optical effective mass of the carriers, the free electron mass, the angular frequency, and the Drude damping time, respectively. The values m_{opt}^*=0.18 and τ_D=1.1 fs for femtosecond-laser-excited silicon were chosen in accordance with the article of Bonse et al [11]. $\varepsilon_r = \mathrm{Re}(\tilde{\varepsilon}^*)/\varepsilon_0$ and $\sigma = \mathrm{Im}(\tilde{\varepsilon}^*)\omega$ were used for the FDTD simulations. For the sake of simplicity, only N_e, the real part n and the imaginary part k of the complex refractive index $\tilde{n}^* = \sqrt{\tilde{\varepsilon}^*}$ are

written here to describe the optical properties when appropriate.

As in [18], the energy absorbed per wavelength below the rough surface was computed as the sum of the electric losses at each time step, that is, $\sigma \Delta t ||\boldsymbol{E}||^2$. When the energy absorbed per wavelength for each Yee cell is constant, the results were analyzed in the frequency domain for different xy planes below the rough surface.

3. Frequency domain notations

Figure 3(a) shows results in the frequency domain of FDTD simulations. The domain is normalized by the norm of the wavevector of the incident laser light that is $2\pi/\lambda$. The random roughness used for this simulation is controlled by a binary function *b(x,y)*. If *b(x,y)*=1, the optical properties of the Yee cell are that of the material, else there is vacuum and *n=1* and *k=0*. The mean of the *b(x,y)* was set to 0.1, which is a value commonly used in the efficacy factor theory [5]. As mentioned in [18], the result, referred to as FDTD-η map, is noisy and it can be difficult to evaluate all the features correctly. A simple method to remove the noise is to average the FDTD-η maps using different *b(x,y)* functions. As an example, such an average of 100 FDTD-η maps is presented in Figure 3(b).

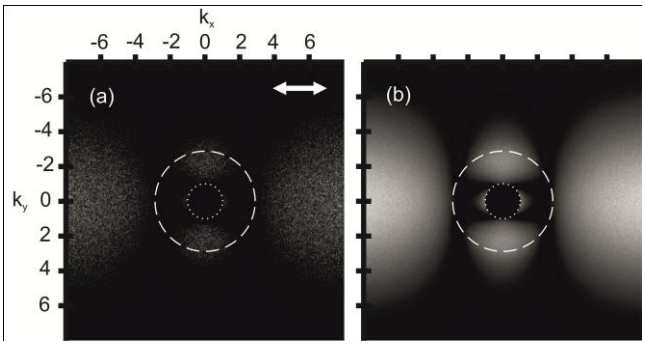

Figure 3: FDTD-η maps computed with N_x=551, N_y=551, N_z=67, Δt=0.04 fs, Δx=40 nm, Δy=40 nm, Δz=20 nm, z=0 nm, $N_e=2\times10^{27}$ m^{-3} n=2.868 and k=0.382. A linear grayscale was used ranging from black (lowest value) to white (highest value). The white arrow indicates the polarization. The dotted circles and dashed circles have radii ||**k**||=1 and ||**k**||=n respectively. (a) Computed with a single surface roughness b(x,y). (b) Computed as an average of 100 FDTD-η maps.

The same notations as in [18] are used here to describe the features present in the frequency domain. For the sake of clarity, the notations are also summarized here. Features present in the figures at ||**k**||>n are referred to as type-r features. They correspond to an energy absorption with a periodicity quite small compared to the laser wavelength. Features intersected by the dashed circle (||**k**||=n) are referred to as type-d. They allow to explain the presence of HSFLs in the direction parallel to the polarization [18]. Along the outer part of the dotted circle (||**k**||=1), the type-s features can be found. They are considered as the trigger of LSFL formation [5][11]. As mentioned in the introduction, this article focus on the explanation of grooves formation in the frame of the electromagnetic approach. Hence, on features in the FDTD-η maps within the ||**k**||=1 circle. In the rest of the article, these features are referred to as type-g. As in [18], type-g features are absent for n=2.868 and k=0.382, and also absent in Figure 3(a) and Figure 3(b). This means that for these optical properties, no LIPSSs with a periodicity larger than the laser wavelength are expected. With $N_e=2\times10^{27}$ m^{-3}, this result was predictable. It was shown in [18] that for these optical properties, LSFL cannot even be produced. Since grooves grow where LSFL have been observed in the early stage [13], it is no surprise that no type-g features are present for $N_e=2\times10^{27}$ m^{-3}. A higher level of excitation is required.

4. Type-g features in FDTD-η maps

In Figure 4, averaged FDTD-η maps, computed with $N_e=4\times10^{27}$ m^{-3}, are shown for different depth z below the rough surface. The same simple roughness model as in the previous section is used. As for Figure 3(b), Figure 4(a) is in good agreement with the non-averaged FDTD-η maps presented in [18]: type-s and type-r features are connected, type-d are almost absent and type-g features start to occur. With increasing depth, type-r merge progressively with type-s features and type-d features start to be more visible and spread progressively within the ||**k**||=n circle. The possible contribution of type-r features on LSFL formation has already been mentioned in [18] and is not discussed here.

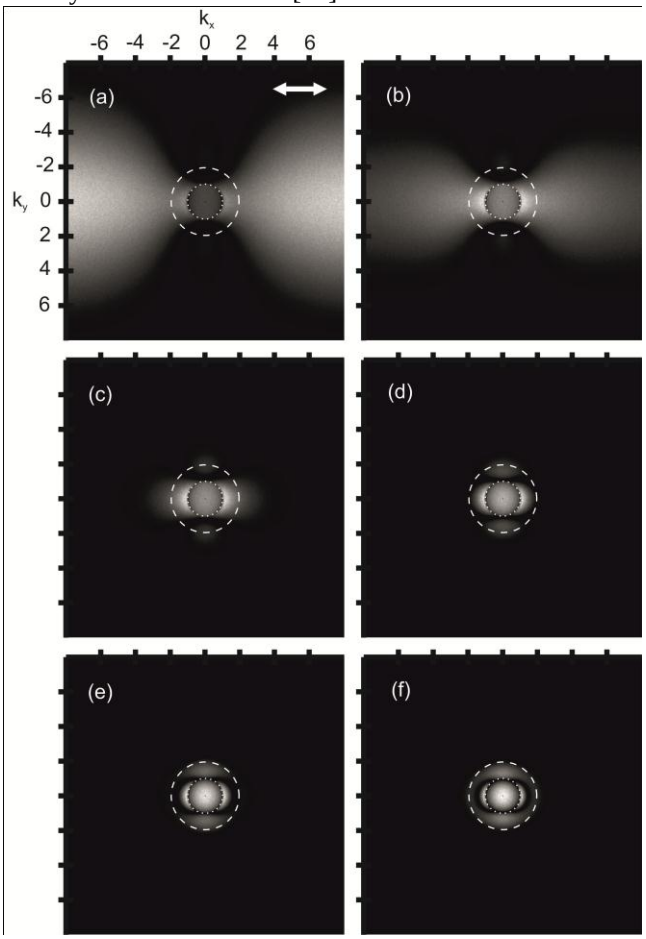

Figure 4: FDTD-η maps computed with N_x=550, N_y=550, N_z=67, Δt=0.04 fs, Δx=40 nm, Δy=40 nm, Δz=20 nm, $N_e=4\times10^{27}$ m^{-3} n=1.943 and k=1.116. A linear grayscale was used ranging from black (lowest value) to white (highest value). The white arrow indicates the polarization. The dotted circles and dashed circles have radiuses ||**k**||=1 and ||**k**||=n respectively. (a) z=0 nm. (b) z=-

40 nm. (c) z=-100 nm. (d) z=-200 nm. (e) z=-300 nm. (f) z=-380 nm.

The maximum amplitude in the frequency domain of the type-g features become comparable to the type-s at about z=-300 nm (Figure 4(e)). These simulations prove that the absorbed energy below a material's rough surface can show a periodicity larger than the wavelength of the polarized light. However, it is unlikely that LIPSSs develop according to an energy pattern present 300 nm below the rough surface. Hence, the type-g features observable in the FDTD-η maps seem unable to explain the growth of grooves on materials. The reason is that the roughness model used by Sipe et al. [7] is not suitable to describe properly the grooves. The *b(x,y)* functions are interesting on a theoretical point of view, because they show flat frequency spectra. Therefore, no frequencies are favored and the FDTD-η maps represent the efficacy with which roughness lead to an inhomogeneous energy absorption at **k**. Nonetheless, more realistic rough surfaces do not have flat frequency spectrums. It is more realistic to use rough surfaces with Gaussian frequency spectrum [22]-[24]. In the following section, the effect of rough surfaces with a Gaussian frequency spectrum on the FDTD-η maps is studied

5. FDTD-η maps and Gaussian frequency spectrum rough surfaces

Rough surfaces, with a Gaussian frequency spectrum, were generated using the approach described in [25]. Only isotropic rough surfaces were investigated. Hence, the rough surfaces used for the FDTD simulations are entirely characterized by the root-mean-square height *h* and the correlation length *l*.

The results of the FDTD simulations in the frequency domain are shown in Figure 5. As in the previous section, the FDTD-η maps have been averaged over 100 rough surfaces. In the left column of Figure 5, the FDTD-η maps are shown just below the rough surfaces, while the averaged spectrum of the rough surfaces is presented in the right column. While type-s features seem uncorrelated to the roughness model, a strong correlation is visible between the rough surfaces spectrum and the type-r and –g features. The larger the correlation length, the more the type-g amplitude increases to the detriment of the type-r features.

It is worth to notice the good agreement of the FDTD-η maps with the efficacy factor theory formula [7]

$$A(\vec{k}) \propto \eta(\vec{k})\left\|b(\vec{k})\right\| \qquad (6)$$

where $A(\mathbf{k})$ is the inhomogeneous energy absorption at z = 0 in the frequency domain, $\eta(\mathbf{k})$ the efficacy factor and $b(\mathbf{k})$ the Fourier component of the roughness. b(**k**) functions with a flat frequency spectrum lead to $A(\mathbf{k}) \propto \eta(\mathbf{k})$. It means that the energy absorption at z = 0 is proportional to the efficacy factor. Hence, the FDTD-η maps presented in Figure 3, Figure 4(a) and [18] are comparable to the efficacy factor graphs. When rough surfaces with Gaussian frequency spectrum are considered, the efficacy factor function is weighted by the spectrum of the rough surface. It is exactly what is observed through Figure 5(a),(c) and (e).

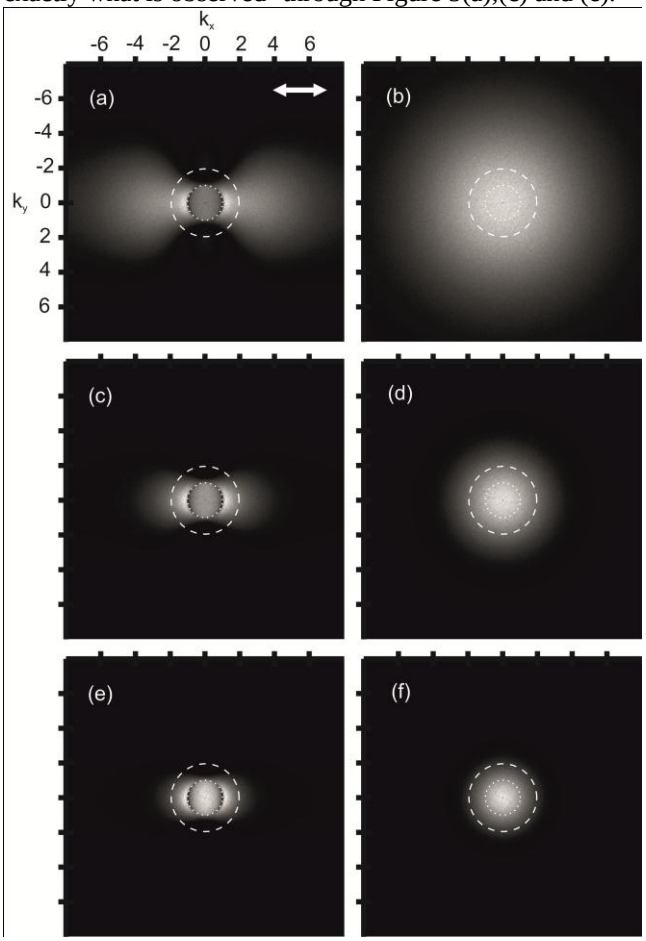

Figure 5: (left column) FDTD-η maps computed with N_x=550, N_y=550, N_z=70, Δt=0.04 fs, Δx=40 nm, Δy=40 nm, Δz=20 nm, z=0 nm, $N_e=4\times10^{27}$ m^{-3} n=1.943 and k=1.116 for different rough surfaces. (right column) averaged spectrum of the rough surfaces. A linear grayscale was used ranging from black (lowest value) to white (highest value). The white arrow indicates the polarization. The dotted circles and dashed circles have radiuses ||**k**||=1 and ||**k**||=n respectively. (a-b) h=12.3±1.5 nm, l=71 nm (c-d) h=13.1±1.6 nm, l=144 nm (e-f) h=13.4±1.8 nm, l=218 nm.

Depending on the rough surface spectrum, type-g features can be of importance at z=0, meaning that the absorbed energy just below a material's rough surface can show a periodicity larger than the wavelength of the laser light. It is now possible to explain the existence of grooves in the frame of the electromagnetic approach. However, it is not clear why grooves can have a preferential direction along the polarization of the laser light as in Figure 1 and in [13]-[15].

In Figure 6, isolines of the FDTD-η map presented in Figure 5(e) have been used to show the shape of the type-g features. The dark blue, turquoise, yellow and red areas are corresponding to frequency values between 0-0.25, 0.25-0.5, 0.5-0.75 and 0.75-1 time the maximum of the FDTD-η map respectively. It should be noticed that the type-g features isolines are not circular but elliptical and the major axis is in the direction orthogonal to the polarization. This mean that if type-g features are the trigger of grooves formation, the grooves should develop in the direction parallel

to the laser polarization. This is actually what is observed in Figure 1 and in [13]-[15].

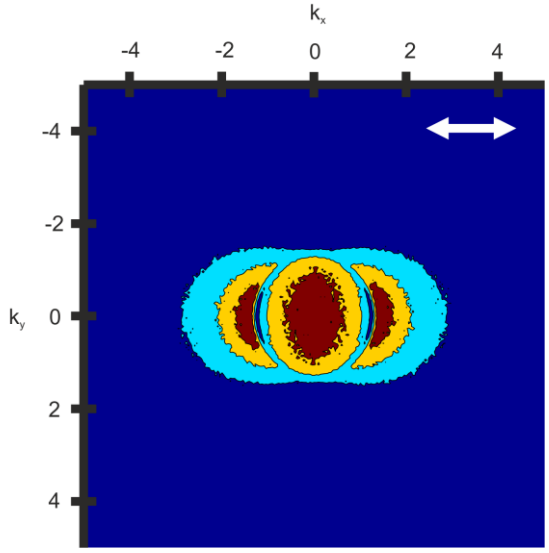

Figure 6: Colored contour of Figure 5(e) ranging from dark blue to red. The isolines were chosen equal to 0, 0.25, 0.5, 0.75 and 1 time the maximum of the FDTD-η map.

6. Conclusion and future work

Based on the approach developed in [18], FDTD simulations have been performed to study the inhomogeneous absorption of laser light below material's rough surfaces. It was shown that grooves and their preferential orientation along the polarization of the laser light can be understood in the frame of the electromagnetic approach of LIPSS formation. In order to get a better understanding of grooves formation, feedback mechanisms leading to LIPSS formation are going to be investigated in future work.

Acknowledgments

This research was carried out under project number M61.3.08300 in the framework of the Research Program of the Materials innovation institute M2i (www.m2i.nl).

References

[1] M. Birnbaum, J. Appl. Phys. 36, 3688 (1965).
[2] M. Siegrist, G. Kaech, and F. Kneubühl, Appl. Phys. A 2, 45 (1973).
[3] Y. Jee, M. F. Becker, and R. M. Walser, J. Opt. Soc. Am. B 5, 648 (1988).
[4] D. C. Emmony, R. P. Howson, and L. J. Willis, Appl. Phys. Lett. 23, 598 (1973).
[5] J. F. Young, J. S. Preston, H. M. van Driel, and J. E. Sipe, Phys. Rev. B 27, 1155 (1983).
[6] P. Temple and M. Soileau, IEEE J. Quantum Electron. 17, 2067 (1981).
[7] J. E. Sipe, J. F. Young, J. S. Preston, and H. M. van Driel, Phys. Rev. B 27, 1141 (1983).
[8] A. Borowiec and H. K. Haugen, Appl. Phys. Lett. 82, 4462 (2003).
[9] Q. Wu, Y. Ma, R. Fang, Y. Liao, Q. Yu, X. Chen, and K. Wang, Appl. Phys. Lett. 82, 1703 (2003).
[10] D. Dufft, A. Rosenfeld, S. K. Das, R. Grunwald, and J. Bonse, J. Appl. Phys. 105, 034908 (2009).
[11] J. Bonse, A. Rosenfeld, and J. Krüger, J. Appl. Phys. 106, 104910 (2009).
[12] M. Huang, F. L. Zhao, Y. Cheng, N. Xu, and Z. Xu, ACS Nano 3, 4062 (2009).
[13] J. Bonse and J. Krüger, J. Appl. Phys. 108, 034903 (2010).
[14] J. Bonse, M. Munz, and H. Sturm, J. Appl. Phys. 97, 013538 (2005).
[15] M. Huang, F. Zhao, Y. Cheng, N. Xu, and Z. Xu, Opt. Express 18, A600 (2010).
[16] F. Costache, S. Kouteva-Arguirova, and J. Reif, Appl. Phys. A 79, 1429 (2004).
[17] J. Reif, F. Costache, M. Henyk, and S. V. Pandelov, Appl. Surf. Sci. 197–198, 891 (2002).
[18] J. Z. P. Skolski, G. R. B. E. Römer, J. V. Obona, V. Ocelik, A. J. Huis in 't Veld, and J. Th. M. De Hosson Phys. Rev. B 85, 075320 (2012)
[19] K. S. Yee, IEEE Trans. Antennas Propag. 14, 302 (1966).
[20] A. Taflove and S. C. Hagness, Computational Electrodynamics: The Finite-Difference Time-Domain Method, 3rd ed. (Artech House, Norwood, 2005).
[21] S. D. Gedney, IEEE Trans. Antennas Propag. 44, 1630 (1996).
[22] A. K. Fung, M. R. Shah, and S. Tjuatja, IEEE Trans. Geosci. Remote Sensing 32, 986-995 (1994)
[23] J. Li, L. X. Guo, and H. Zeng, Waves Random Complex Media 19(3), 418-429 (2009).
[24] L. Kuang and Y.Q. Jin, IEEE Trans Antennas Propag. 55(8) 2302-2312 (2007).
[25] Y. Kuga, and P. Phu, Prog. Electromagn. Res. PIER, 14, 37-88 (1996)